Environmental Science & Technology

pubs.acs.org/est

Article

# Cadmium Isotope Fractionation during Adsorption and Substitution with Iron (Oxyhydr)oxides

Xinran Yan, Mengqiang Zhu, Wei Li, Caroline L. Peacock, Jingyuan Ma, Hanjie Wen, Fan Liu, Zhengbing Zhou, Chuanwei Zhu,* and Hui Yin*

Cite This: *Environ. Sci. Technol.* 2021, 55, 11601−11611

Read Online

ACCESS | Metrics & More | Article Recommendations | Supporting Information

**ABSTRACT:** Cadmium (Cd) isotopes have great potential for understanding Cd geochemical cycling in soil and aquatic systems. Iron (oxyhydr)oxides can sequester Cd via adsorption and isomorphous substitution, but how these interactions affect Cd isotope fractionation remains unknown. Here, we show that adsorption preferentially enriches lighter Cd isotopes on iron (oxyhydr)oxide surfaces through equilibrium fractionation, with a similar fractionation magnitude ($\Delta^{114/110}Cd_{solid\text{-}solution}$) for goethite (Goe) (−0.51 ± 0.04‰), hematite (Hem) (−0.54 ± 0.10‰), and ferrihydrite (Fh) (−0.55 ± 0.03‰). Neither the initial $Cd^{2+}$ concentration or ionic strength nor the pH influence the fractionation magnitude. The enrichment of the light isotope is attributed to the adsorption of highly distorted [$CdO_6$] on solids, as indicated by Cd K-edge extended X-ray absorption fine-structure analysis. In contrast, Cd incorporation into Goe by substitution for lattice Fe at a Cd/Fe molar ratio of 0.05 preferentially sequesters heavy Cd isotopes, with a $\Delta^{114/110}Cd_{solid\text{-}solution}$ of 0.22 ± 0.01‰. The fractionation probably occurs during the transformation of Fh into Goe via dissolution and reprecipitation. These results improve the understanding of the Cd isotope fractionation behavior being affected by iron (oxyhydr)oxides in Earth's critical zone and demonstrate that interactions with minerals can obscure anthropogenic and natural Cd isotope characteristics, which should be carefully considered when applying Cd isotopes as environmental tracers.

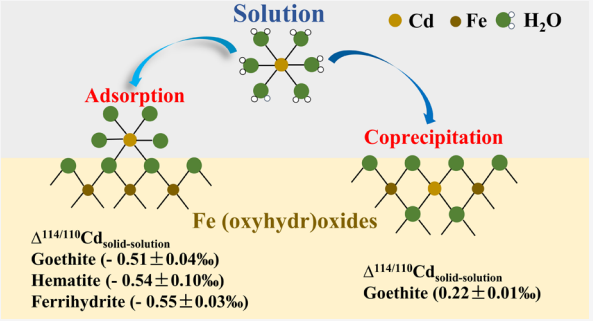


**KEYWORDS:** *metal (oxyhydr)oxides, heavy-metal isotopes, adsorption, coprecipitation, mineral transformation, extended X-ray absorption fine structure spectroscopy*



## INTRODUCTION

Cadmium (Cd) is a highly toxic and carcinogenic heavy metal for humans without a safe exposure limit.[1−3] Risk prediction and remediation of anthropogenic Cd pollution in terrestrial environments require a fundamental understanding of its geochemical cycling. Recently, Cd isotope signatures have been increasingly applied to understand biogeochemical reactions and fingerprint Cd sources and fate in contaminated ecosystems.[4−9] However, this promise is hampered as multiple processes can cause heavy-metal isotope fractionation, such as adsorption onto mineral surfaces,[9,10] coprecipitation with minerals,[11,12] complexation by inorganic[13] or organic ligands,[14,15] membrane protein transport in plants,[16] and weathering.[9,17] Among these processes, adsorption and coprecipitation on mineral surfaces or structural incorporation into mineral lattices are of much importance, which are the well-known association mechanisms of heavy metals with minerals, particularly for Cd, Zn, and Ni.[10,18−30]

Metal isotope fractionation during adsorption onto mineral surfaces can be affected by mineral phases, pH, ionic strength (IS), surface loading, and reaction time. Following an equilibrium isotope fractionation, Zn adsorbed onto Fe (oxyhydr)oxides is enriched in heavy isotopes; and the fractionation magnitude on ferrihydrite (Fh) is stronger than that on goethite (Goe).[20] In synthetic seawater, birnessite (a Mn oxide) also retains heavy Zn isotopes, with the fractionation magnitude decreasing with increasing surface loading or decreasing IS.[31] Light Ni isotopes are preferentially adsorbed onto Fe (oxyhydr)oxides with the fractionation magnitude on Goe being much larger than that on Fh.[19,21] Finally for Cd, birnessite was reported to preferentially adsorb light Cd isotopes, with the fractionation magnitude increasing with increasing IS but decreasing with the reaction time.[10]

Metal incorporation into the mineral structure can also induce isotope fractionation, generally following a kinetic fractionation mechanism. Incorporation of Zn into the calcite lattice during coprecipitation preferentially enriches heavy

Received: October 14, 2020
Revised: July 28, 2021
Accepted: July 29, 2021
Published: August 9, 2021

isotopes.[32] Additionally, the isotope fractionations of metal may behave inversely when interacting with different minerals. Heavy Ni isotopes incorporate into birnessite layers as a result of adsorption at pH 8.2;[22] however, its coprecipitation with Fh shows indistinguishable fractionations from that caused by adsorption, that is, enriching light isotopes in the solids.[19] During Cd precipitation with sulfur (S), light Cd isotopes are sequestered in CdS.[12] Substitution of Cd for calcite lattice Ca during the crystal growth in freshwater does not lead to Cd isotope fractionation but in artificial seawater light Cd isotopes are enriched in solids.[11,33,34]

According to the isotope fractionation theory,[35] heavy isotopes tend to be concentrated in chemical species, forming the stiffest bonds with short bond lengths. Heavier Zn isotopes in $[ZnO_4]$ compared to $[ZnO_6]$ during Zn adsorption onto Fe/Mn (oxyhydr)oxides can be well explained by the substantially shorter Zn−O bond length in the former.[18,20,31] Formation of Zn inner sphere complexes on kaolinite edge sites at high pH and IS results in a larger fractionation than that during the formation of outer sphere complexes on the basal planes at low pH and IS.[29] Additionally, the distortion of the metal octahedron after adsorption makes the metal−O bond less stiff and can also lead to the enrichment of light isotopes.[10,19] Furthermore, in solution, complexation by inorganic or organic ligands can induce fractionation among various aqueous species, which have different adsorption behaviors on mineral surfaces and thus affect the overall isotope fractionation.[36] Theoretical calculations showed that successively increasing the number of water molecules of the Cd hydration complexes from 4 to 6 favors heavy isotopes. Replacement of the coordinated water molecules around the metal by Cl and S gradually makes the complexes lighter but O or N makes the complexes heavier[13,14,37−39] (Table S1).

Iron (oxyhydr)oxides are common minerals found in soils and sediments and mediate the geochemical behaviors of metal pollutants, especially in tropical and subtropical regions. Despite the fact that Cd is primarily associated with Fe (oxyhydr)oxides in these environments,[9,40] no study so far has investigated the Cd isotope fractionation behavior during adsorption and structural incorporation. The objectives of the present study are to determine (1) the direction and magnitude of Cd isotope fractionation during adsorption on different Fe (oxyhydr)oxides [Goe, hematite (Hem), and Fh], (2) the effects of pH, IS, and initial Cd concentrations on adsorption-induced fractionation, and (3) the Cd isotope fractionation during incorporation into Goe.

## MATERIALS AND METHODS

**Reagents.** All the reagents were used as received, and detailed information about them is provided in the Supporting Information. The Cd isotopic composition of $Cd(NO_3)_2 \cdot 4H_2O$ used for the Cd-doped Goe synthesis is 0.48 ± 0.01‰ relative to the NIST SRM 3108 Cd standard (std) according to eq 1

$$\delta^{114/110}\mathrm{Cd} = \left[\frac{(^{114}\mathrm{Cd}/^{110}\mathrm{Cd})_{\mathrm{sample}}}{(^{114}\mathrm{Cd}/^{110}\mathrm{Cd})_{\mathrm{std}}} - 1\right] \times 1000 \quad (1)$$

while the Cd ICP standard used for the adsorption experiments has a $\delta^{114/110}$Cd of −1.71 ± 0.04‰.

**Synthesis and Characterization of Iron (Oxyhydr)-oxides.** Two-line Fh (2LFh), Goe, and Hem were synthesized according to Cornell and Schwertmann (2003).[41] Fh was synthesized by adding 330 mL of 1 M KOH solution to 500 mL of 0.1 M $Fe(NO_3)_3 \cdot 9H_2O$ solution with a drop rate of 1 mL·min$^{-1}$ under stirring until the solution pH reached 7−8, and then the pH was maintained for 1 h by the addition of KOH solution. Goe was synthesized by adding 180 mL of 5 M KOH solution to 100 mL of 1 M $Fe(NO_3)_3 \cdot 9H_2O$ solution. The obtained suspension was diluted to 2 L with ultrapure water under stirring, and then sealed, and aged at 70 °C for 60 h after the pH was adjusted to >13. Hem was synthesized by slowly adding 60 mL of 1 M $Fe(NO_3)_3 \cdot 9H_2O$ solution to 750 mL of boiling ultrapure water at a rate of 0.5 mL·min$^{-1}$ under stirring. After synthesis, the solids were centrifuged, freeze-dried, and then stored at 4 °C. The purity of the obtained solids was confirmed by powder X-ray diffraction (XRD) (Figure S1 and Table S2), while the sample morphologies were measured by electron microscopy (Figures S2, S3, and Table S3). Goe, Hem, and 2LFh have $N_2$-BET specific surface areas of 37, 56, and 256 m$^2$·g$^{-1}$ and points of zero charge (PZCs) of ∼9.7, ∼9.8, and ∼8.5, respectively (Figure S4).

**Coprecipitation Experiments.** Cd−Fe coprecipitates were obtained by adding $Cd(NO_3)_2$ into the $Fe(NO_3)_3$ solution in acid-cleaned 1 L Teflon bottles and adjusting the pH to >13 prior to aging at 70 °C. After aging for 12 and 60 h, 50 mL of the solid and supernatant were collected. The obtained solids were named 5CdGoe_12h and 5CdGoe_60h. These solids were subsequently treated with 50 mL of 0.2 M oxalic acid for 2 h to remove poorly crystalline phases. The as-obtained solids were labeled 5CdGoe_12h_o and 5CdGoe_60h_o. Then, these solids were further treated with 50 mL of 0.4 M $HNO_3$ for 0.5 h to remove small Goe particles and/or $Cd^{2+}$ adsorbed on mineral surfaces.[27] The finally obtained solids were named 5CdGoe_12h_n and 5CdGoe_60h_n. The detailed procedure is depicted in Figure S5a. Quantitative phase analysis of the solids was conducted using TOPAS software (DIFFRAC$^{plus}$ TOPAS version 4.2, Bruker-AXS)[27] (Figure S5c). The obtained solids and supernatants were used for the Cd isotope analysis.

**Adsorption Experiments.** For adsorption kinetics, 22.2, 44.5, or 89 μM $Cd^{2+}$ was reacted with 1 g·L$^{-1}$ Goe or Hem, or 0.5 g·L$^{-1}$ 2LFh in 0.05 M $KNO_3$ at pH 7 for 48 h, and aliquot suspensions were collected at the predetermined time intervals (Table S4). Adsorption edges were measured over pH 4−8 for 24 h (Table S5). Adsorption isotherms were carried out with initial $Cd^{2+}$ concentrations of 0−89.0 μM for Goe or Hem and 0−177.9 μM for 2LFh at pH 7 for 24 h (Tables S5 and S6). Prior to mixing with the $Cd^{2+}$ solution, the solids were hydrated in the background electrolyte for 24 h. Low (0.05 M) and high (0.36 M) IS were used to determine the IS effects on $Cd^{2+}$ adsorption and associated isotope fractionation, and $NO_3^-$ was used rather than $Cl^-$ because the former is more common in soil and aquatic systems.

In all the experiments, $Cd^{2+}$ was added to the mineral suspensions to obtain a similar surface coverage but prevent Cd precipitation.[42] The suspension pH was maintained via adding 1 M $HNO_3$ or KOH. At the end of the reactions, the solids and solutions were separated through 0.2 μm cellulose membranes. To remove the dissolved Cd, the selected Cd-loaded solids (Table S7) were immediately washed sequentially with a background electrolyte and ultrapure water, the pH of which were adjusted to that used for adsorption experiments.[20] The cleaned solid (labeled CdMineral_initial Cd concentration_reaction pH) was collected with membrane filtration, sealed with Kapton tape, and stored at 4 °C within


https://doi.org/10.1021/acs.est.0c06927
Environ. Sci. Technol. 2021, 55, 11601−11611

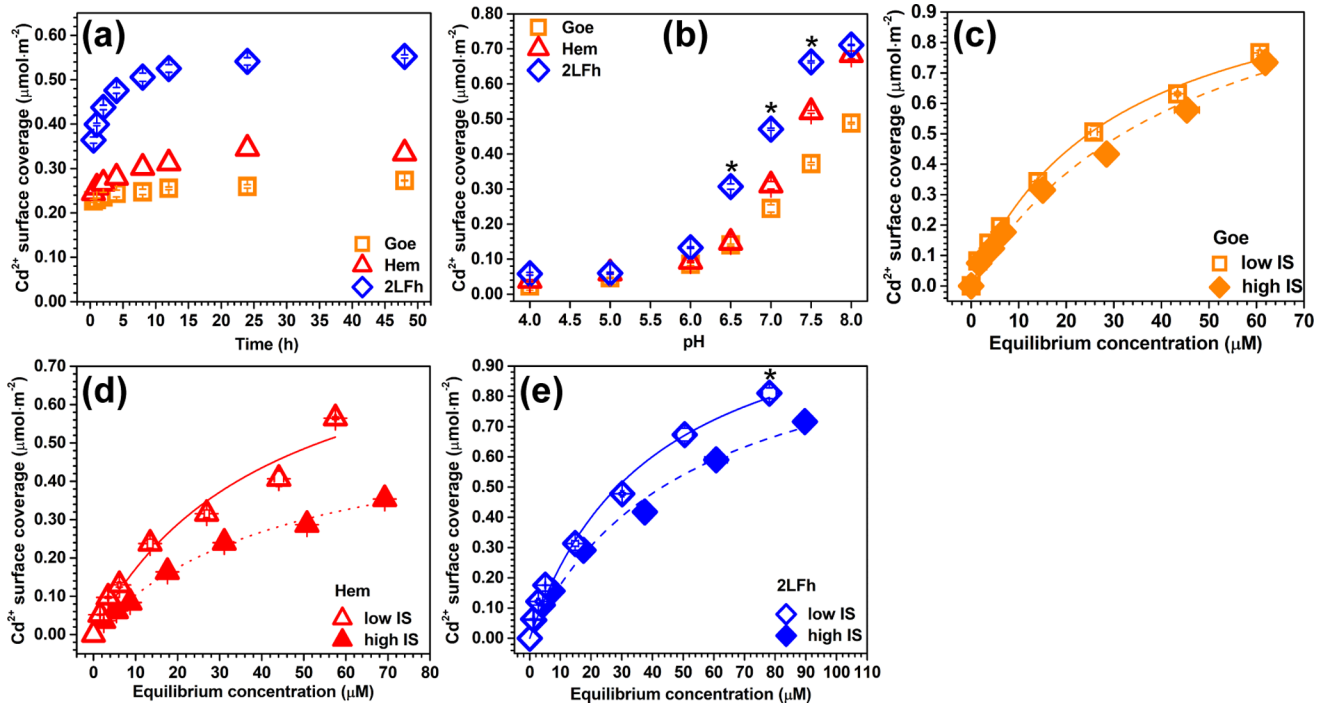


**Figure 1.** Macroscopic adsorption behavior of $Cd^{2+}$ on Goe, Hem, and 2LFh at different reaction conditions. (a) Adsorption kinetics at pH 7 ± 0.05 with a duration time of 48 h. (b) Sorption edges. The Cd initial concentrations ($[Cd^{2+}]$) were set as 22.2, 44.5, and 89.0 $\mu$M for Goe, Hem, and 2LFh, respectively, in both kinetic and sorption-edge experiments, with a background electrolyte of 0.05 M $KNO_3$ solution. Adsorption isotherm curves at low and high IS conditions (IS: 0.05 and 0.36 M $KNO_3$ solution, respectively) at pH 7 ± 0.05 for (c) Goe, (d) Hem, and (e) 2LFh, with $[Cd^{2+}]$ = 0−89.0 $\mu$M for Goe and Hem and $[Cd^{2+}]$ = 0−177.9 $\mu$M for 2LFh. Symbols are experimental data, and lines are Langmuir fits. All the experiments were conducted using a solid/solution ratio of 1 g·$L^{-1}$ for Goe and Hem and 0.5 g·$L^{-1}$ for 2LFh at 25 ± 2 °C. In (b,e), the samples indicated by asterisk (*) were selected for Cd K-edge EXAFS analysis.

24 h prior to Cd K-edge-extended X-ray absorption fine-structure (EXAFS) analysis. For the isotope analysis, experiments of the selected pH edge and isotherms (Table S8) were re-conducted in acid-cleaned Teflon vials in the same way as described above.

The Cd concentrations in solutions and solids after digestion were determined using a flame or graphite furnace atomic absorption spectrometer (FAAS or GFAAS, Agilent Technologies 200 Series AA or GTA 120 Graphite Tube Atomizer), depending on Cd concentrations. The detection limit for FAAS is 6.77 $\mu$g·$L^{-1}$ and the uncertainty is 0.3%, while those for GFAAS are 0.06 $\mu$g·$L^{-1}$ and 2.7%, respectively. Control experiments with no $Cd^{2+}$ addition to the Goe suspension gave a Cd concentration of 7.35 ± 0.07 $\mu$g·$L^{-1}$ by FAAS. As the latter value was substantial, it was subtracted from the sample Cd concentrations. Duplicate or triplicate experiments were carried out to ensure reproducibility.

**Cadmium Isotope Analysis.** The sample solutions were evaporated and the solids of the coprecipitation and adsorption experiments (with membrane) were digested prior to isotope analysis.

About 600 ng of Cd of each sample was weighed and placed into Teflon beakers and then mixed with 0.6 mL of 1 mg·$L^{-1}$ $^{111}Cd$−$^{110}Cd$ double spike solution to achieve a Cd spike−sample ratio of ∼1. Detailed information on the double spike solution, sample digestion, and Cd chemical purification was reported in our previous studies,[43,44] and the Cd recovery rate was >95% for all the samples.

Cadmium isotopic ratios were measured using a Thermo Scientific Neptune plus MC-ICP-MS with a Ni "Standard" sampler and Ni "x-type" skimmer cones at the State Key Laboratory of Ore Deposit Geochemistry, Institute of Geochemistry, CAS. A nebulizer−spray chamber (with an uptake rate of ∼50 $\mu$L·$min^{-1}$) was used as the sample introduction system, and the low-resolution entrance slit was chosen throughout the analysis. The instrumental baseline and peak center were obtained before each sample (standard) analysis. Each measurement included 60 integrations of 4.194 s in 2 blocks of 30 cycles, and we also measured $^{105}Pd$ at every start of 10 cycles with integrations of 2.097 s, followed by 120 s of washing with 5% $HNO_3$ to lower the Cd signal to the original background level (<0.1 mV). The instrumental sensitivity was about 28 V/ppm. In this study, the double spike method was employed to correct the mass bias. All the samples and bracketing reference solutions were diluted to 400 ng·$mL^{-1}$ [sample (200 ng·$mL^{-1}$) + double spike (200 ng·$mL^{-1}$)] within a 10% difference.[45]

Using a MATLAB-based script and the measured double-spike data, Cd isotope compositions of the samples and standards were calculated.[43] The NIST SRM 3108 Cd (lot no. 130116) was used as a zero reference standard. The JMC (lot no.74-075219k) and Nancy Spex Cd solution (CRPG, France), as well as a solid Cd isotope reference (NOD-P-1, manganese-nodule), were additionally used as secondary reference standards. The measured values for JMC Cd ($\delta^{114/110}Cd$ = −1.68 ± 0.08‰; 2SD, $n$ = 4), Nancy Spex Cd ($\delta^{114/110}Cd$ = −0.11 ± 0.06‰; 2SD, $n$ = 4), and NOD-P-1 ($\delta^{114/110}Cd$ = 0.13 ± 0.08‰; 2SD, $n$ = 2) agreed well with previous results.[43,46] The long-term reproducibility of this method was better than ±0.08‰ (2SD; $N$ = 20) with $\delta^{114/110}Cd_{Nancy-Spex}$ values ranging from −0.08 to −0.15‰. The isotopic fractionation of Cd ($\Delta^{114/110}Cd_{solid\text{-}solution}$)


https://doi.org/10.1021/acs.est.0c06927
Environ. Sci. Technol. 2021, 55, 11601−11611

**Table 1. Fitting results of EXAFS Spectra for Model Compounds and Typical Cd Adsorption and Coprecipitation Samples, Including a Third Cumulant (Cum.) in the Fit of the First Cd−O Coordination Shell to Account for the Asymmetry in a Non-Gaussian Model**

| sample | path | CN | $R$ (Å) | $\sigma^2$ (Å$^2$) | third cum. | $\Delta E$ (eV) | $\chi^2$ | $R$-factor[a] |
|---|---|---|---|---|---|---|---|---|
| $Cd(NO_3)_2$ | Cd−O | 6.6 ± 0.6 | 2.29 ± 0.02 (2.27 ± 0.01)[b] | 0.0086 ± 0.0010 | 0.0003 ± 0.0004 | 3.3 ± 1.7 | 41.82 | 0.0058 |
| $Cd(OH)_2$[c] | Cd−O | 7.4 ± 1.1 | 2.31 ± 0.02 (2.30 ± 0.01) | 0.0090 ± 0.0018 | 0.0004 ± 0.0005 | 6.5 ± 1.4 | 3510.01 | 0.0177 |
| | Cd−Cd | 10.2 ± 2.7 | 3.51 ± 0.01 | 0.0117 ± 0.0021 | | | | |
| CdFh_10_pH6.5[d] | Cd−O | 6.2 ± 0.7 | 2.30 ± 0.03 (2.24 ± 0.01) | 0.0118 ± 0.0014 | 0.0011 ± 0.0006 | 2.4 ± 2.1 | 2.00 | 0.0119 |
| | Cd−Fe | 0.7 ± 0.4 | 3.31 ± 0.02 | 0.0029 ± 0.0047 | | | | |
| CdFh_10_pH7[d] | Cd−O | 7.4 ± 1.0 | 2.31 ± 0.04 (2.26 ± 0.01) | 0.0143 ± 0.0020 | 0.0010 ± 0.0008 | 4.1 ± 2.4 | 45.89 | 0.0195 |
| | Cd−Fe | 4.7 ± 1.3 | 3.33 ± 0.05 | 0.0282 ± 0.0165 | | | | |
| CdFh_20_pH7[d] | Cd−O | 5.7 ± 1.2 | 2.28 ± 0.05 (2.24 ± 0.01) | 0.0086 ± 0.0024 | 0.0007 ± 0.0009 | 3.2 ± 3.9 | 22.62 | 0.0482 |
| | Cd−Fe | 0.7 ± 0.3 | 3.33 ± 0.04 | 0.0030[e] | | | | |
| CdFh_10_pH7.5[d] | Cd−O | 5.8 ± 0.7 | 2.32 ± 0.03 (2.26 ± 0.01) | 0.0106 ± 0.0014 | 0.0011 ± 0.0006 | 5.2 ± 2.1 | 18.82 | 0.0139 |
| | Cd−Fe | 0.8 ± 1.0 | 3.36 ± 0.03 | 0.0097 ± 0.0101 | | | | |
| 5CdGoe_60h_n | Cd−O | 6.4 ± 1.6 | 2.29 ± 0.06 (2.22 ± 0.02) | 0.0085 ± 0.0031 | 0.0013 ± 0.0012 | 7.6 ± 4.4 | 56.20 | 0.0675 |
| | Cd−Fe | 0.4 ± 0.9 | 3.07 ± 0.04 | 0.0004 ± 0.0168 | | | | |

[a]$R$ indicates the fitting quality, which is calculated by the equation: $R = \sum(k^3\chi_{obs}(k) - k^3\chi_{cal}(k))^2/\sum(k^3\chi_{obs}(k))^2$. [b]These values in the bracket were those derived from the first Cd−O shell fitting without the addition of the third cumulant. [c]This standard was adopted from our previous study.[27] [d]These samples were named CdMineral_initial Cd concentration_reaction pH, and the isotope compositions of these samples were measured. [e]This parameter was fixed during the fitting.

between the adsorbed phase and the aqueous phase is defined as eq 2

$$\Delta^{114/110}Cd_{solid\text{-}solution} = \delta^{114/110}Cd_{solid} - \delta^{114/110}Cd_{solution} \quad (2)$$

**EXAFS Data Collection and Analysis.** The Cd K-edge EXAFS spectra were collected on a beamline BL14W1 at the Shanghai Synchrotron Radiation Facility (SSRF) at room temperature.[27] Cadmium-containing samples (0.9−4.4 wt % Cd) and 50 mM $Cd(NO_3)_2$ solution were measured with a Si(311) double-crystal monochromator in the fluorescence mode, while $\beta$-$Cd(OH)_2$ in the transmission mode. A silver metal foil was used for energy calibration (25,529 eV). The data processing was performed using IFEFFIT software.[47] The parameters for the background removal were the following: $E_0$ = 26,714 eV, $k$-weight = 2, and $R_{bkg}$ = 1.0. Structural parameters ($R$, CN, and $\sigma^2$) were obtained by fitting the experimental $k^3$-weighted spectra to the standard equation.[48] FEFF7 was used to calculate the phase and amplitude functions for single-scattering paths,[49] based on the structure models of Cd-doped Goe (ICSD 71810) and Fh (ICSD 158475). An amplitude reduction factor ($S_0^2$) of 0.95 was adopted from a previous study.[50] During EXAFS analysis, the first Cd−O shell fitting was conducted assuming a Gaussian or a non-Gaussian distribution model, with a third cumulant in the latter to account for the asymmetry of the [$CdO_6$] octahedron.[51,52] More details are provided in the Supporting Information.

## RESULTS

**Macroscopic $Cd^{2+}$ Adsorption Behavior.** Iron (oxyhydr)oxides have high adsorption reactivity toward $Cd^{2+}$. The adsorption edges, kinetics, and isotherms show similar patterns for the three mineral phases (Figure 1). Adsorption occurs rapidly initially and then increases slowly during the first 12 h. After 24 h, pseudo-equilibria are reached, and the Cd adsorption densities remain almost constant. After 48 h, the $Cd^{2+}$ adsorption density on 2LFh is 1.7−2 times that on Hem or Goe (Figure 1a), owing to the higher initial $Cd^{2+}$ concentration and lower mineral concentration (Table S4). With increasing pH, $Cd^{2+}$ adsorption increases slightly below pH 6.0 but dramatically over pH 6.0−8.0 (Figure 1b, Table S5), a characteristic of $Cd^{2+}$ adsorption on Fe (oxyhydr)-oxides.[53−55] Further, $Cd^{2+}$ adsorption increases with increasing initial $Cd^{2+}$ concentration (Figure 1c−e). The maximum $Cd^{2+}$ adsorption densities obtained by the Langmuir isotherm fitting are 1.12 and 1.23 $\mu$mol·m$^{-2}$ for Goe, 0.89 and 0.57 $\mu$mol·m$^{-2}$ for Hem, and 1.21 and 1.10 $\mu$mol·m$^{-2}$ for 2LFh at low and high IS, respectively (Table S6).

**Cadmium Binding Environments in the Adsorbed and Coprecipitated Samples.** The $k^3$-weighted Cd K-edge EXAFS spectra and the corresponding Fourier transforms of Cd-loaded 2LFh samples are distinct from those of the $Cd(NO_3)_2$ solution and $\beta$-$Cd(OH)_2$ (Figure S6), indicating the formation of inner sphere complexes on 2LFh surfaces without the precipitation of Cd hydroxide. For the adsorption samples, including a third cumulant in the first shell of the EXAFS fitting (Figure S6 and Table 1) improves the fitting quality by reducing $\chi^2$ and the $R$-factor by 5−42% compared to that without a third cumulant (Figure S7 and Table S6). Thus, a third cumulant is included for the spectral fitting of all the samples and standards. The EXAFS fitting demonstrates an average Cd−O distance of 2.29 ± 0.02 Å in the $Cd(NO_3)_2$ solution, consistent with previously reported values.[24,56,57] $\beta$-$Cd(OH)_2$ has a Cd−O bond length of 2.31 ± 0.02 Å in the [$CdO_6$] unit and an edge-sharing Cd−Cd distance of 3.51 ± 0.01 Å, which also agree with literature values.[25,27] For the Cd-adsorbed 2LFh samples, the Cd−O distances are 2.28−2.32 Å. Only one Cd−Fe shell with distances ranging from 3.31−3.36 Å is needed to fit the $R + \Delta R \sim 2.9$ Å peak, suggesting $Cd^{2+}$ mainly exists as bidentate edge-sharing complexes.[24] Moreover, these distances are almost constant independent of pH or surface loading, suggesting the formation of the same type of surface complexes.

Transmission electron microscopy (TEM) and powder XRD analyses show that the Cd−Fe coprecipitates aging at 70 °C for 12 and 60 h are the mixtures of Fh and Goe. An XRD quantitative phase analysis shows that 5CdGoe_12h and 5CdGoe_60h contain 76.1 ± 2.3% and 7.1 ± 2.5% Fh, respectively (Figure S5c). The oxalate removes all the Fh and


https://doi.org/10.1021/acs.est.0c06927
Environ. Sci. Technol. 2021, 55, 11601−11611

subsequent $HNO_3$ treatment removes $Cd^{2+}$ adsorbed on Goe surfaces, yielding pure Cd-doped Goe (Figure S5b,c). The oxalate treatment removes 84.9 ± 0.8% Cd and 84.3 ± 0.4% Fe from 5CdGoe_12h and 27.9 ± 0.2% Cd and 14.1 ± 0.1% Fe from 5CdGoe_60h (Figure S5a). These contents of Fe dissolved are consistent with the Fh proportions determined by XRD analysis. The $HNO_3$ treatment removes 12.7 ± 0.1% Cd and 12.8 ± 0.0% Fe from Fe5CdGoe_12h_o and 2.2 ± 0.0% Cd and 1.0 ± 0.0% Fe from 5CdGoe_60h_o (Figure S5a). All the solids obtained have a Cd/Fe molar ratio of ~0.05. The lattice parameters of Cd-doped Goe determined by Rietveld structure refinement[58] are expanded compared to those of Goe (Table S2), suggesting the incorporation of Cd into the Goe lattice.[27,59] This is further confirmed by EXAFS analysis. The EXAFS oscillation of 5CdGoe_60h_n has a special feature at ~6.4 $Å^{-1}$ (array in Figure S6A), a characteristic of Cd-doped Goe.[25,57] The EXAFS fitting indicates a Cd−O distance of 2.29 ± 0.06 Å and a Cd−Fe distance of 3.07 ± 0.04 Å. The later distance corresponds to the Cd−Fe pairs between edge-sharing $[CdO_6]$ and $[FeO_6]$ units along the *c* axis in the Cd-doped Goe structure.[25,60]

**Isotopic Behavior of $Cd^{2+}$ during Adsorption on Fe (Oxyhydr)oxides.** The isotopic compositions ($\delta^{114/110}Cd$) of dissolved and adsorbed $Cd^{2+}$ during the isotherm adsorption indicate that light Cd isotopes are preferentially adsorbed on the solids (Figures 2, S8a−c and Table S8). The isotope fractionations ($\Delta^{114/110}Cd_{solid\text{-}solution}$) vary from −0.63 ± 0.02‰ to −0.47 ± 0.03‰ for Goe and from −0.45 ± 0.05‰ to −0.35 ± 0.06‰ for 2LFh at low IS. While IS affects the $Cd^{2+}$ adsorption density on Hem (Figure 1), the isotope fractionations at low (−0.55 ± 0.11‰, $n$ = 7) and high IS (−0.52 ± 0.06‰, $n$ = 3) are statistically the same. pH does not affect the fractionation magnitude either (Figures 2, S8d−f, and S9).

The $\delta^{114/110}Cd$ values represented as a function of Cd adsorbed fractions ($f$) are used to identify whether isotopic equilibrium is attained between the adsorbed and aqueous $Cd^{2+}$ (Figure 2). Both the equilibrium models, where the adsorbed Cd isotopically exchanges with aqueous Cd in a closed system (eq 3), and the Rayleigh model, where the adsorbed Cd is isolated from the isotopic exchange (eq 4), were used to fit the data

$$\delta^{114/110}Cd_{solution} = \frac{\delta^{114/110}Cd_{stock} - 1000 \cdot f \cdot (\alpha_{solid\text{-}solution} - 1)}{1 - f + (f \cdot \alpha_{solid\text{-}solution})} \quad \text{(equilibrium model)} \tag{3}$$

$$\delta^{114/110}Cd_{solution} = (1000 + \delta^{114/110}Cd_{stock}) \cdot (1 - f)^{(\alpha_{solid\text{-}solution} - 1)} - 1000 \quad \text{(Rayleigh model)} \tag{4}$$

where $\alpha_{solid\text{-}solution}$ denotes the isotope fractionation factor between the dissolved and adsorbed Cd and $\delta^{114/110}Cd_{stock}$ is the measured value for the stock solution.

The equilibrium model fits the data much better than the Rayleigh model, confirming an equilibrium isotopic exchange process (Figure 2). The fractionation factors, obtained by averaging the two values determined from $\delta^{114/110}Cd$ in solution and in solid separately using the equilibrium model, are 0.99949 ± 0.00004, 0.99946 ± 0.00010, and 0.99945 ± 0.00003 for Goe, Hem, and 2LFh, respectively. According to

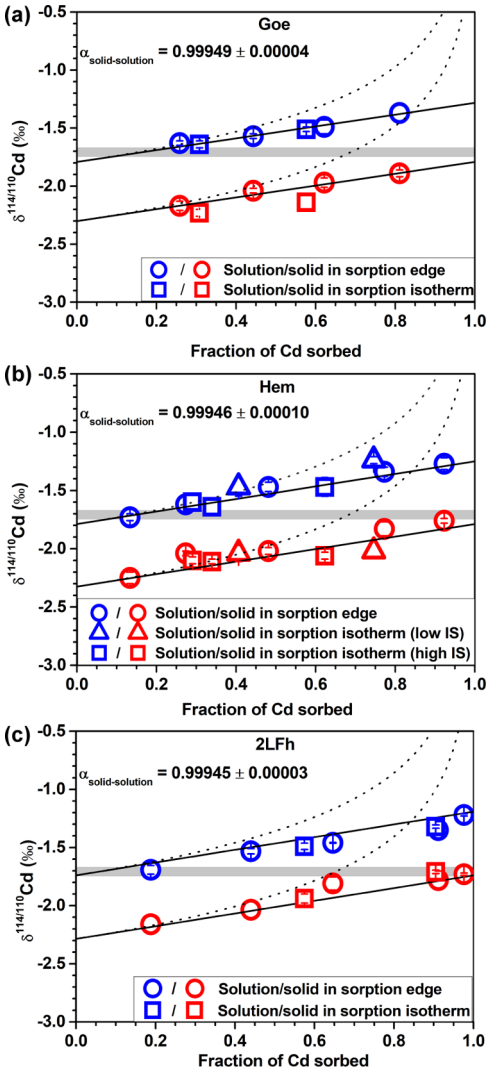


**Figure 2.** Cd isotope compositions between solution and solid phases as the function of Cd-adsorbed fraction during adsorption onto Goe (a), Hem (b), and 2LFh (c). The solid lines and dashed curves represent the theoretical $\delta^{114/110}Cd$ values calculated using the equilibrium model and the Rayleigh model, respectively. The fractionation factor ($\alpha_{solid\text{-}solution}$) given is the average of the two values determined using $\delta^{114/110}Cd$ in solution and in the solid separately using the equilibrium model. The $Cd^{2+}$ stock solution used for adsorption experiments has a $\delta^{114/110}Cd$ value of −1.71 ± 0.04‰ (gray line in each panel).

$\alpha_{solid\text{-}solution}$, the isotopic fractionation between the adsorbed and dissolved Cd can be calculated using eq 5

$$\Delta^{114/110}Cd_{solid\text{-}solution} \cong 1000 \times \ln \alpha_{solid\text{-}solution} \tag{5}$$

The theoretical $\Delta^{114/110}Cd_{solid\text{-}solution}$ values are −0.51 ± 0.04‰, −0.54 ± 0.10‰, and −0.55 ± 0.03‰ for Goe, Hem, and 2LFh, respectively.

**Isotopic Behavior during $Cd^{2+}$ Coprecipitation with Goe.** The isotope composition analysis (Figure 3) demonstrates that $\delta^{114/110}Cd_{soild\text{-}solution}$ of 5CdGoe_12h and solution are 0.44 ± 0.07‰ and 0.64 ± 0.08‰, respectively. After aging for an additional 48 h, the $\delta^{114/110}Cd$ for 5CdGoe_60h becomes 0.50 ± 0.03‰, while that in the solution substantially decreases to 0.24 ± 0.01‰. After the oxalate treatment of 5CdGoe_60h, $\delta^{114/110}Cd$ in the solution (oxalate) decreases to


https://doi.org/10.1021/acs.est.0c06927
Environ. Sci. Technol. 2021, 55, 11601−11611

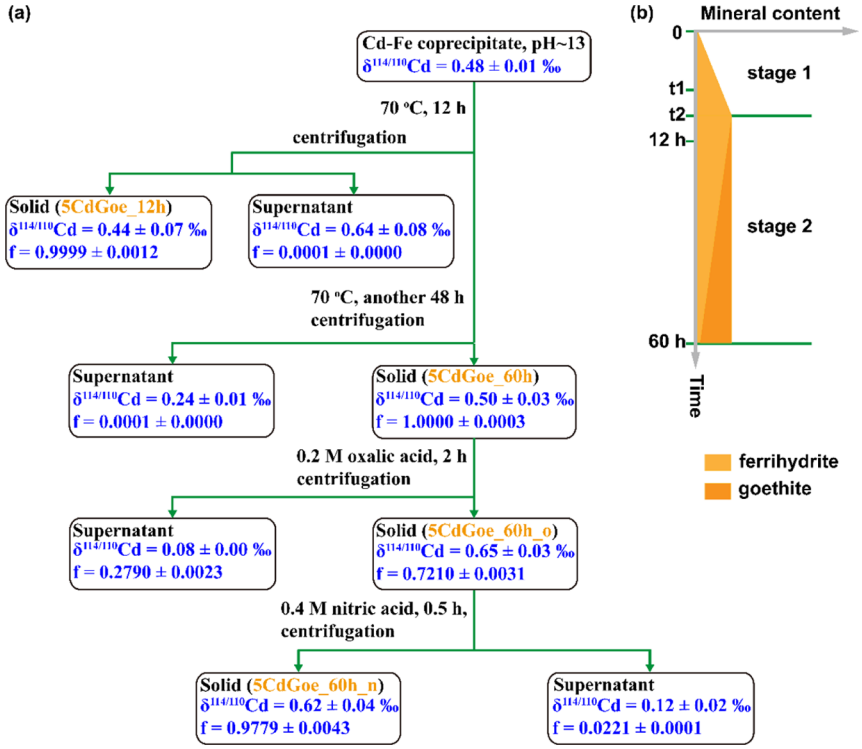


**Figure 3.** (a) Illustration of Cd isotope mass balance during Cd-doped Goe synthesis. Cadmium isotope composition and the fraction of Cd (f) in each part were added. (b) Corresponding changes in the contents of Fh and Goe with time. Time $t_1$ refers to the time taken for removing the kinetic isotope fractionation of Cd, while $t_2$ refers to the time taken for completing the Fh crystallization.

0.08 ± 0.00‰, while that in the solid (5CdGoe_60h_o) increases to 0.65 ± 0.03‰. The subsequent $HNO_3$ treatment of 5CdGoe_60h_o results in a slight increase of $\delta^{114/110}$Cd in the solution ($HNO_3$) and an almost unchanged $\delta^{114/110}$Cd (0.62 ± 0.04‰) in the obtained 5CdGoe_60h_n.

Further, the isotope fractionation magnitude during Cd incorporation into the Goe lattice was calculated. Because all Cd is transferred to the solid (Figures 3a and S5a), the isotope signals recorded during this process are listed in eqs 6 and 7

$$\delta^{114/110}\mathrm{Cd}_{\text{stock-solution}} = f_1 \times \delta^{114/110}\mathrm{Cd}_{\text{adsorbed\_Fh}} + f_2 \times \delta^{114/110}\mathrm{Cd}_{\mathrm{HNO_3}} + f_3 \times \delta^{114/110}\mathrm{Cd}_{\text{5CdGoe\_60h\_n}} \quad (6)$$

$$\Delta^{114/110}\mathrm{Cd}_{\text{stock-solution}} = 0 = f_1 \times \Delta^{114/110}\mathrm{Cd}_{\text{adsorbed\_Fh}} + f_2 \times \Delta^{114/110}\mathrm{Cd}_{\mathrm{HNO_3}} + f_3 \times \Delta^{114/110}\mathrm{Cd}_{\text{5CdGoe\_60h\_n}} \quad (7)$$

where $f_1$, $f_2$, and $f_3$ are the fractions of Cd adsorbed on the Fh phase that was removed by the oxalate treatment of 5CdGoe_60h, adsorbed on the Goe surfaces that were removed by the $HNO_3$ treatment of 5CdGoe_60h_o, and that incorporated into the 5CdGoe_60h_n mineral lattice, respectively. However, based on the mass balance for 5CdGoe_60h, $f_2$ (1.59 ± 0.01%) is negligible. The $\delta^{114/110}\mathrm{Cd}_{\text{adsorbed\_Fh}}$ is 0.08 ± 0.00‰, and the adsorption-induced Cd fractionation on 2LFh (−0.55 ± 0.03‰) determined in the adsorption experiments can be used for $\Delta^{114/110}\mathrm{Cd}_{\text{adsorbed\_Fh}}$. Based on eqs 6 and 7, the $\delta^{114/110}\mathrm{Cd}_{\text{5CdGoe\_60h\_n}}$ and $\Delta^{114/110}\mathrm{Cd}_{\text{5CdGoe\_60h\_n}}$ are calculated to be 0.65 ± 0.01‰ and 0.22 ± 0.01‰, of which the former agrees well with the measured value for 5CdGoe_60h_n (Figures 3a and S5a). All these results clearly confirm that the incorporation of Cd into the Goe lattice substantially enriches heavy Cd isotopes.

## DISCUSSION

**Cadmium Isotope Fractionation During Adsorption onto Iron (Oxyhydr)oxides.** Heavy isotopes are generally enriched in substances with stronger bonds and shorter bond lengths,[10,35] such as the enrichment of heavy Zn and Cu isotopes on solids during adsorption on Fe and Al (oxyhydr)-oxides.[20,61] In contrast, the present study shows the preferential adsorption of light $Cd^{2+}$ isotopes onto Fe (oxyhydr)oxides. A similar phenomenon was observed for $Ni^{2+}$ adsorption on Fe oxides,[19] in which the distortion of adsorbed [$NiO_6$] was proposed to account for the apparent anomaly. [$CdO_6$] distortion during adsorption on manganite was also previously proposed based on EXAFS analysis.[52] The present Cd K-edge EXAFS fittings with the third cumulant greatly improve the fit quality compared to that without the third cumulant and both demonstrate almost the same structural parameters for $Cd(NO_3)_2$ or $\beta$-$Cd(OH)_2$, confirming the regular [$CdO_6$] structure.[52] However, the first Cd−O shell distances in the Cd-adsorbed samples derived from fitting with a third cumulant (2.28−2.32 Å) are substantially longer than those obtained without a third cumulant (2.24−2.26 Å). Additionally, the third cumulants, which are measures of disorder,[52] for Cd-sorbed samples (0.0007−0.0011) are larger than those for $Cd(NO_3)_2$ and $\beta$-$Cd(OH)_2$ (0.0003−0.0004). We thus conclude that [$CdO_6$] adsorbed on these Fe (oxyhydr)oxide surfaces is highly distorted (Table 1), which


https://doi.org/10.1021/acs.est.0c06927
Environ. Sci. Technol. 2021, 55, 11601−11611

probably accounts for the enrichment of the light Cd isotope on the solids.

The fractionation magnitude of Zn or Ni during adsorption on Fe (oxyhydr)oxides depends on the mineral phases involved.[20,21] In contrast, our results show that Cd adsorptions on Goe, Hem, and 2LFh result in the same fractionation magnitude. The differences in isotope fractionations for Cd compared to Zn and Ni during adsorption on Fe (oxyhydr)-oxides can be understood by considering their different metal adsorption mechanisms. For example, the tetrahedral coordination of adsorbed Zn on Fh results in a larger Zn fractionation than during the octahedral coordination of adsorbed Zn on Goe,[20] whereas a stronger Ni complexation on Fh than on Goe results in smaller Ni fractionation by Fh than by Goe.[21] However, in comparison with the first-row transition metals, $Cd^{2+}$ may be more prone to form outer sphere complexes.[15,62,63] IS affects Cd adsorption on the three Fe (oxyhydr)oxides with a stronger effect on Hem than on Goe and 2LFh, suggesting the possible formation of outer sphere complexes on Hem. The Cd inner sphere complexes formed on Hem are probably also different from those on Goe and 2LFh. Indeed, the geometry of adsorbed Cd on 2LFh, as measured in the present study, is similar to those of adsorbed Cd on Goe reported previously.[24,25,64−66] No EXAFS information for Cd adsorption on Hem is available yet. However, crystallographic studies demonstrate that Goe needles and Hem cubic particles expose different facets, which have different surface charge properties, and thus possess different cation adsorption characteristics.[67−69] Though both outer and inner spherical complexation of Cd can induce isotope fractionations,[15,29] the observed same Cd isotope fractionation magnitude on these Fe (oxyhydr)oxides clearly suggest that the types of Cd binding complexes do not impact the final isotope fractionations.

Further, though high IS suppresses Cd adsorption on Hem, the Cd isotope fractionation magnitude on Hem at high and low IS conditions are almost the same, which is different from that during Zn and Cd adsorption onto Mn oxides.[10,31] Calculations of aqueous Cd speciation at low-and high-$KNO_3$ concentrations using Visual MINTEQ 3.1[70] indicate Cd occurs dominantly as $Cd(H_2O)_6^{2+}$ (86%) with 13% $Cd(NO_3)(H_2O)_5^{+}$ at low IS, and $Cd(H_2O)_6^{2+}$ and $Cd(NO_3)(H_2O)_5^{+}$ are almost equal (48% vs 45%) at high IS. However, the reduced partition function ratios $10^3 \ln(\beta_{114-110})$ for $Cd(NO_3)(H_2O)_5^{+}$ and $Cd(H_2O)_6^{2+}$ are almost similar (2.323 ± 0.034 vs 2.299 ± 0.028) (Table S1),[13] thus the increase in the proportion of the former with increasing IS has almost no effect on the Cd isotope fractionation magnitude during adsorption on Hem. This suggests that the changes in aqueous speciation also have no effect on the final Cd isotope fractionation. Conclusively, during $Cd^{2+}$ adsorption onto these Fe (oxyhydr)oxides, the fractionation magnitude and the fractionation mechanism [($CdO_6$) distortion] are independent of the types of Cd-binding sites on minerals and environmental conditions.

**Cadmium Isotope Fractionation during Coprecipitation with Goe.** Almost all Cd is retained in 5CdGoe_12h and 5CdGoe_60h, thus the $\delta^{114/110}$Cd of these solids are equal to the Cd stock solution (0.48 ± 0.01‰) (Figures 3 and S5a). The oxalate treatment of 5CdGoe_60h removes all the Cd associated with Fh. This leads to the decrease of the $\delta^{114/110}$Cd value in the resulting solution, which is consistent with the expected fractionation as this part of Cd is probably adsorbed on Fh[27] and thus has a large negative fractionation according to the results of the adsorption-induced Cd isotope fractionation on Fh (Figure 2). Further treating 5CdGoe_60-h_o with $HNO_3$ removes Cd adsorbed on Goe particles.[27] The extracted solution is enriched in light isotopes compared to 5CdGoe_60h_o. This is also consistent with the expected fractionation as the Cd adsorbed on Goe is enriched in light isotopes (Figure 2).

Several studies have reported isotope fractionation induced by metal incorporation into mineral structures. This may predominantly involve two mechanisms: preferential retention of one species in the mineral after isotopic exchange equilibrium among various aqueous species and direct preferential enrichment of one aqueous isotope owing to, for example, coordination chemistry differences or kinetic effects. Light Cd isotopes are enriched in the solid during CdS precipitation, which is controlled by the isotope equilibrium between aqueous Cd species.[12] During Cd incorporation into calcite in artificial seawater, light isotopes are preferred in the solid following a kinetic isotope effect, ascribing to the retardation of crystal growth and Cd uptake caused by the overwhelming occupancy of the active surface sites by the major ions (particularly $Na^+$ and $K^+$).[11] Recently, aqueous $Zn^{2+}$ was reported to first adsorb onto calcite growth sites by forming tetrahedral inner sphere complexes enriching heavy isotopes and then incorporate into the crystal lattice by increasing the coordination number to 6 without further isotope fractionation.[34]

We obtain a $\Delta^{114/110}Cd_{solid\text{-}solution}$ of ∼0.22‰ for the incorporation of Cd into the Goe structure. Goe formation from Fh likely involves the formation of reactive and labile small Fh particles and subsequent dissolution to provide dissolved $Fe^{3+}$ for Goe crystallization in the bulk solution,[41,71−73] which can be divided into two stages (Figure 3b):

In stage 1 (0-$t_2$ in Figure 3b), coprecipitation of Cd with Fe at a high $OH^-$ concentration probably sequesters all the Cd and Fe into Fh at time $t_2$.[73] The $\delta^{114/110}$Cd of the "absolutely pure" Fh should be ∼0.48‰, while that in the corresponding equilibrium solution should be larger than 0.64‰. The enrichment of heavy isotopes in this solution probably results from a kinetic isotope effect in that the presence of 0.45 M $K^+$ in the initial reactant blocks the active sites on the primary Fe (oxyhydr)oxide nanoparticles, and lighter isotopes are adsorbed faster by the solids.[11,73] However, this kinetic effect is progressively removed within a few hours ($t_1$ in Figure 3b).[10] Further, the formed Fh particles greatly adsorb light Cd isotopes through the whole stage 1 (0-$t_2$ in Figure 3b) and thus leave heavy isotopes in solutions, according to the results of Cd isotope fractionation during adsorption experiments (Figure 2).

Subsequently, stage 2 ($t_2$-60 h in Figure 3b) starts. Fh particles slowly dissolve, releasing soluble Fe and Cd species into the solution. The Cd released is expected to be relatively heavy isotopically, based on the fact that many weathering processes of Cd-containing minerals preferentially release heavy isotopes into the fluids[4,17,46] and that the remaining Fh retains light isotopes. As the dissolved Fe units $\{[Fe(OH)_4]^-\}$[41,73] nucleate and grow into less soluble Goe, monovalent Cd species $\{[Cd(OH)_3]^-\}$ in solution, which are the most suitable growth units[41] and enrich heavy isotopes,[13] interact with the Goe growth sites via ion-by-ion attachment.[34] This leads to the enrichment of heavy Cd isotopes in the Goe structures. The slow dissolution of Fh results in the coexistence


https://doi.org/10.1021/acs.est.0c06927
Environ. Sci. Technol. 2021, 55, 11601−11611

of Goe and Fh particles in this stage. This is confirmed by the powder XRD quantitative phase analysis and TEM of 5CdGoe_12h and 5CdGoe_60h (Figure S5b,c). The part of Cd associated with Fh particles in these solids is probably enriched in light isotopes, as evidenced by the isotope composition of the resulting solution after treatment of 5CdGoe_60h with oxalate (Figure 3a). In contrast, the Goe particles in the solids during this stage retain heavy Cd isotopes. This is convincingly supported by the isotope composition analysis of 5CdGoe_60h_o and 5CdGoe_60h_n (Figure 3a), which are pure Cd-doped Goe crystals (Figure S5b,c).

In conclusion, the enrichment of heavy Cd isotopes in Cd-doped Goe crystals is achieved probably during the Fh dissolution−Goe crystallization processes. Though the enrichment of heavy isotopes by incorporation into the Mn oxide structure is also observed for Ni, the fractionation magnitude is not given.[22] All these results suggest that the incorporation of octahedrally coordinated cations into Fe/Mn (oxyhydr)oxides enriches heavier isotopes relative to solutions. Nonetheless, the metal isotope fractionation behaviors and mechanisms in these processes are worthy of further study.

## ■ ENVIRONMENTAL IMPLICATIONS

The cadmium isotope composition reflects Cd geochemical cycling and helps track Cd anthropogenic sources.[3,16,74,75] However, based on previous research with other metals, interactions with minerals are likely to affect Cd isotope compositions in environmental systems. To the best of our knowledge, the present study is the first to investigate Cd isotope fractionation during adsorption on and isomorphous substitution in Fe (oxyhydr)oxides. The preferential adsorption of light Cd isotopes onto Fe (oxyhydr)oxides, as well as on Mn oxides[10] and humic acids,[15] explains the enrichment of light isotopes in soils and sediments relative to the fluids.[3,4,9,46,76] Considering the high abundance of Fe (oxyhydr)oxides in tropical and subtropical soils,[9,40] they probably play an important role in controlling Cd isotope characteristics as other soil components, for example, clays, Mn oxides, and organic matter. Our results suggest that the enrichment of lighter Cd isotopes in Fe−Mn nodules in the lower layers of soil profiles compared to the surrounding soils observed previously[9] is likely to be caused by the enrichment of light Cd isotopes on Goe surfaces in the nodules. Our study also suggests that Fe (oxyhydr)oxide transformation between different phases can also result in Cd isotope fractionation. These geochemical processes greatly complicate the potential use of Cd isotopes to identify Cd sources.[9,77] Our results are consistent with the recently proposed Fh dissolution−Goe crystallization mechanism and suggest that metal isotope fractionation behavior by adsorption or coprecipitation with minerals provides insights into mineral transformation pathways and mechanisms that are hard to elucidate with other techniques.[73] Future studies are warranted, including the coprecipitation of different heavy metals with Fe minerals and investigation into the effects of prolonged aging, ligands, and temperatures.

## ■ ASSOCIATED CONTENT

### Supporting Information

The Supporting Information is available free of charge at https://pubs.acs.org/doi/10.1021/acs.est.0c06927.

Reagent information; summary of bond lengths, coordination numbers, and reduced partition function ratios for typical metals ($Cd^{2+}$, $Zn^{2+}$, and $Ni^{2+}$) in complexes with $H_2O$ (free hydrated ion), and typical inorganic ligands ($Cl^-$, $NO_3^-$, $HS^-$, and $OH^-$); powder XRD, chemical composition, zeta potential, TEM and SEM analyses of obtained minerals; illustration of experimental schedules for isotope fractionation analysis during $Cd^{2+}$ coprecipitation with Goe; $Cd^{2+}$ macroscopic adsorption data for kinetic, adsorption edge, and isotherms; details on Cd K-edge EXAFS data collection and analysis, and the EXAFS fitting results; and Cd isotope compositions in solid and aqueous phases, mass balance, and fractionation (PDF)

## ■ AUTHOR INFORMATION


### Corresponding Authors

**Chuanwei Zhu** − *State Key Laboratory of Ore Deposit Geochemistry, Institute of Geochemistry, Chinese Academy of Sciences, Guiyang 550002, China*; Email: zhuchuanwei@mail.gyig.ac.cn

**Hui Yin** − *Key Laboratory of Arable Land Conservation (Middle and Lower Reaches of Yangtse River), Ministry of Agriculture and Rural Affairs, College of Resources and Environment, Huazhong Agricultural University, Wuhan 430070, China; State Environmental Protection Key Laboratory of Soil Health and Green Remediation, Ministry of Ecology and Environment, Huazhong Agricultural University, Wuhan 430070, China;* orcid.org/0000-0003-3060-7025; Phone: +86 27 87280271; Email: yinhui666@mail.hzau.edu.cn; Fax: +86 27 87288618

### Authors

**Xinran Yan** − *Key Laboratory of Arable Land Conservation (Middle and Lower Reaches of Yangtse River), Ministry of Agriculture and Rural Affairs, College of Resources and Environment, Huazhong Agricultural University, Wuhan 430070, China; State Environmental Protection Key Laboratory of Soil Health and Green Remediation, Ministry of Ecology and Environment, Huazhong Agricultural University, Wuhan 430070, China*

**Mengqiang Zhu** − *Department of Ecosystem Science and Management, University of Wyoming, Laramie, Wyoming 82071, United States;* orcid.org/0000-0003-1739-1055

**Wei Li** − *Key Laboratory of Surficial Geochemistry, Ministry of Education, School of Earth Sciences and Engineering, Nanjing University, Nanjing 210023, China;* orcid.org/0000-0002-0789-0320

**Caroline L. Peacock** − *School of Earth and Environment, University of Leeds, Leeds LS2 9JT, U.K.*

**Jingyuan Ma** − *Shanghai Synchrotron Radiation Facility, Shanghai Institute of Applied Physics, Chinese Academy of Sciences, Shanghai 201204, China*

**Hanjie Wen** − *State Key Laboratory of Ore Deposit Geochemistry, Institute of Geochemistry, Chinese Academy of Sciences, Guiyang 550002, China*

**Fan Liu** − *Key Laboratory of Arable Land Conservation (Middle and Lower Reaches of Yangtse River), Ministry of Agriculture and Rural Affairs, College of Resources and Environment, Huazhong Agricultural University, Wuhan 430070, China; State Environmental Protection Key Laboratory of Soil Health and Green Remediation, Ministry*

*of Ecology and Environment, Huazhong Agricultural University, Wuhan 430070, China;* orcid.org/0000-0003-0341-923X

**Zhengbing Zhou** − *State Key Laboratory of Nuclear Resources and Environment, East China University of Technology, Nanchang 330013, China*

Complete contact information is available at: https://pubs.acs.org/10.1021/acs.est.0c06927

### Notes

The authors declare no competing financial interest.

## ■ ACKNOWLEDGMENTS

The authors greatly thank the Associate Editor Prof. Dr. T. David Waite and Dr. Damien Guinoiseau and other three anonymous reviewers for their thoughtful comments and suggestions. Prof. Susan H. Little at University College London, Dr. Wenxian Gou at Nanjing University, and Lena Chen at University of Leeds are gratefully thanked for their helpful comments and discussions. Prof. Alain Manceau at ISTerre, Université Grenoble Alpes-CNRS is also gratefully thanked for helpful discussions on $Cd^{2+}$ adsorption on goethite. The authors gratefully thank the Natural Science Foundations of China (nos. 41771267 and 42077015), the National Key Research and Development Program of China (no. 2016YFD0800403), Key Science and Technology Projects of Inner Mongolia autonomous region (no. 2019ZD001), and the Fundamental Research Funds for the Central Universities (grant 103-510320036) for financial support. This work was financially supported by the Royal Society Newton Mobility grant (IEC/NSFC/191423). C.L.P. gratefully acknowledges the Royal Society Wolfson Research Merit Award (WRM/FT/170005).

## ■ REFERENCES

(1) Janssen, D. J.; Abouchami, W.; Galer, S. J. G.; Purdon, K. B.; Cullen, J. T. Particulate cadmium stable isotopes in the subarctic northeast Pacific reveal dynamic Cd cycling and a new isotopically light Cd sink. *Earth Planet. Sci. Lett.* **2019**, *515*, 67−78.

(2) Godt, J.; Scheidig, F.; Grosse-Siestrup, C.; Esche, V.; Brandenburg, P.; Reich, A.; Groneberg, D. A. The toxicity of cadmium and resulting hazards for human health. *J. Occup. Med. Toxicol.* **2006**, *1*, 22.

(3) Zhou, J.-W.; Li, Z.; Liu, M.-S.; Yu, H.-M.; Wu, L.-H.; Huang, F.; Luo, Y.-M.; Christie, P. Cadmium isotopic fractionation in the soil−plant system during repeated phytoextraction with a cadmium hyperaccumulating plant species. *Environ. Sci. Technol.* **2020**, *54*, 13598−13609.

(4) Imseng, M.; Wiggenhauser, M.; Keller, A.; Müller, M.; Rehkämper, M.; Murphy, K.; Kreissig, K.; Frossard, E.; Wilcke, W.; Bigalke, M. Fate of Cd in agricultural soils: A stable isotope approach to anthropogenic impact, soil formation, and soil-plant cycling. *Environ. Sci. Technol.* **2018**, *52*, 1919−1928.

(5) Chrastný, V.; Čadková, E.; Vaněk, A.; Teper, L.; Cabala, J.; Komárek, M. Cadmium isotope fractionation within the soil profile complicates source identification in relation to Pb−Zn mining and smelting processes. *Chem. Geol.* **2015**, *405*, 1−9.

(6) Yang, W.-J.; Ding, K.-B.; Zhang, P.; Qiu, H.; Cloquet, C.; Wen, H.-J.; Morel, J.-L.; Qiu, R.-L.; Tang, Y.-T. Cadmium stable isotope variation in a mountain area impacted by acid mine drainage. *Sci. Total Environ.* **2019**, *646*, 696−703.

(7) Salmanzadeh, M.; Hartland, A.; Stirling, C. H.; Balks, M. R.; Schipper, L. A.; Joshi, C.; George, E. Isotope tracing of long-term cadmium fluxes in an agricultural soil. *Environ. Sci. Technol.* **2017**, *51*, 7369−7377.

(8) Barraza, F.; Moore, R. E. T.; Rehkämper, M.; Schreck, E.; Lefeuvre, G.; Kreissig, K.; Coles, B. J.; Maurice, L. Cadmium isotope fractionation in the soil−cacao systems of Ecuador: a pilot field study. *RSC Adv.* **2019**, *9*, 34011−34022.

(9) Gao, T.; Liu, Y.; Xia, Y.; Zhu, J.-M.; Wang, Z.; Qi, M.; Liu, Y.; Ning, Z.; Wu, Q.; Xu, W.; Liu, C. Cadmium isotope compositions of Fe-Mn nodules and surrounding soils: Implications for tracing Cd sources. *Fund. Res.* **2021**, *1*, 269.

(10) Wasylenki, L. E.; Swihart, J. W.; Romaniello, S. J. Cadmium isotope fractionation during adsorption to Mn oxyhydroxide at low and high ionic strength. *Geochim. Cosmochim. Acta* **2014**, *140*, 212−226.

(11) Horner, T. J.; Rickaby, R. E. M.; Henderson, G. M. Isotopic fractionation of cadmium into calcite. *Earth Planet. Sci. Lett.* **2011**, *312*, 243−253.

(12) Guinoiseau, D.; Galer, S. J. G.; Abouchami, W. Effect of cadmium sulphide precipitation on the partitioning of Cd isotopes: Implications for the oceanic Cd cycle. *Earth Planet. Sci. Lett.* **2018**, *498*, 300−308.

(13) Yang, J.; Li, Y.; Liu, S.; Tian, H.; Chen, C.; Liu, J.; Shi, Y. Theoretical calculations of Cd isotope fractionation in hydrothermal fluids. *Chem. Geol.* **2015**, *391*, 74−82.

(14) Zhao, Y.; Li, Y.; Wiggenhauser, M.; Yang, J.; Sarret, G.; Cheng, Q.; Liu, J.; Shi, Y. Theoretical isotope fractionation of cadmium during complexation with organic ligands. *Chem. Geol.* **2021**, *571*, 120178.

(15) Ratié, G.; Chrastný, V.; Guinoiseau, D.; Marsac, R.; Vaňková, Z.; Komárek, M. Cadmium isotope fractionation during complexation with humic acid. *Environ. Sci. Technol.* **2021**, *55*, 7430.

(16) Wiggenhauser, M.; Aucour, A.-M.; Bureau, S.; Campillo, S.; Telouk, P.; Romani, M.; Ma, J. F.; Landrot, G.; Sarret, G. Cadmium transfer in contaminated soil-rice systems: Insights from solid-state speciation analysis and stable isotope fractionation. *Environ. Pollut.* **2021**, *269*, 115934.

(17) Zhu, C.; Wen, H.; Zhang, Y.; Yin, R.; Cloquet, C. Cd isotope fractionation during sulfide mineral weathering in the Fule Zn-Pb-Cd deposit, Yunnan Province, Southwest China. *Sci. Total Environ.* **2018**, *616−617*, 64−72.

(18) Gou, W.; Li, W.; Ji, J.; Li, W. Zinc isotope fractionation during sorption onto Al oxides: Atomic level understanding from EXAFS. *Environ. Sci. Technol.* **2018**, *52*, 9087−9096.

(19) Wasylenki, L. E.; Howe, H. D.; Spivak-Birndorf, L. J.; Bish, D. L. Ni isotope fractionation during sorption to ferrihydrite: Implications for Ni in banded iron formations. *Chem. Geol.* **2015**, *400*, 56−64.

(20) Juillot, F.; Maréchal, C.; Ponthieu, M.; Cacaly, S.; Morin, G.; Benedetti, M.; Hazemann, J. L.; Proux, O.; Guyot, F. Zn isotopic fractionation caused by sorption on goethite and 2-Lines ferrihydrite. *Geochim. Cosmochim. Acta* **2008**, *72*, 4886−4900.

(21) Gueguen, B.; Sorensen, J. V.; Lalonde, S. V.; Peña, J.; Toner, B. M.; Rouxel, O. Variable Ni isotope fractionation between Fe-oxyhydroxides and implications for the use of Ni isotopes as geochemical tracers. *Chem. Geol.* **2018**, *481*, 38−52.

(22) Sorensen, J. V.; Gueguen, B.; Stewart, B. D.; Peña, J.; Rouxel, O.; Toner, B. M. Large nickel isotope fractionation caused by surface complexation reactions with hexagonal birnessite. *Chem. Geol.* **2020**, *537*, 119481.

(23) Yuan, Q.; Li, P.; Liu, J.; Lin, Y.; Cai, Y.; Ye, Y.; Liang, C. Facet-dependent selective adsorption of Mn-doped $\alpha$-$Fe_2O_3$ nanocrystals toward heavy-metal ions. *Chem. Mater.* **2017**, *29*, 10198−10205.

(24) Tiberg, C.; Gustafsson, J. P. Phosphate effects on cadmium(II) sorption to ferrihydrite. *J. Colloid Interface Sci.* **2016**, *471*, 103−111.

(25) Spadini, L.; Manceau, A.; Schindler, P. W.; Charlet, L. Structure and stability of $Cd^{2+}$ surface complexes on ferric oxides: 1. Results from EXAFS spectroscopy. *J. Colloid Interface Sci.* **1994**, *168*, 73−86.

(26) Singh, B.; Gräfe, M.; Kaur, N.; Liese, A. Chapter 8 - Applications of Synchrotron-Based X-Ray Diffraction and X-Ray Absorption Spectroscopy to the Understanding of Poorly Crystalline

and Metal-Substituted Iron Oxides. In *Developments in Soil Science*; Balwant, S., Markus, G., Eds.; Elsevier, 2010; Vol. *34*, pp 199−254.
(27) Liu, L.; Wang, X.; Zhu, M.; Ma, J.; Zhang, J.; Tan, W.; Feng, X.; Yin, H.; Liu, F. The speciation of Cd in Cd−Fe coprecipitates: Does Cd substitute for Fe in goethite structure? *ACS Earth Space Chem.* **2019**, *3*, 2225−2236.
(28) Yin, H.; Wu, Y.; Hou, J.; Yan, X.; Li, Z.; Zhu, C.; Zhang, J.; Feng, X.; Tan, W.; Liu, F. Preference of Co over Al for substitution of Fe in goethite ($\alpha$-FeOOH) structure: Mechanism revealed from EXAFS, XPS, DFT and linear free energy correlation model. *Chem. Geol.* **2020**, *532*, 119378.
(29) Guinoiseau, D.; Gélabert, A.; Moureau, J.; Louvat, P.; Benedetti, M. F. Zn isotope fractionation during sorption onto kaolinite. *Environ. Sci. Technol.* **2016**, *50*, 1844−1852.
(30) Mo, X.; Siebecker, M. G.; Gou, W.; Li, L.; Li, W. A review of cadmium sorption mechanisms on soil mineral surfaces revealed from synchrotron-based X-ray absorption fine structure spectroscopy: Implications for soil remediation. *Pedosphere* **2021**, *31*, 11−27.
(31) Bryan, A. L.; Dong, S.; Wilkes, E. B.; Wasylenki, L. E. Zinc isotope fractionation during adsorption onto Mn oxyhydroxide at low and high ionic strength. *Geochim. Cosmochim. Acta* **2015**, *157*, 182−197.
(32) Mavromatis, V.; González, A. G.; Dietzel, M.; Schott, J. Zinc isotope fractionation during the inorganic precipitation of calcite − Towards a new pH proxy. *Geochim. Cosmochim. Acta* **2019**, *244*, 99−112.
(33) DePaolo, D. J. Surface kinetic model for isotopic and trace element fractionation during precipitation of calcite from aqueous solutions. *Geochim. Cosmochim. Acta* **2011**, *75*, 1039−1056.
(34) Xie, X.; Yan, L.; Li, J.; Guan, L.; Chi, Z. Cadmium isotope fractionation during Cd-calcite coprecipitation: Insight from batch experiment. *Sci. Total Environ.* **2021**, *760*, 143330.
(35) Schauble, E. A. Applying stable isotope fractionation theory to new systems. *Rev. Mineral. Geochem.* **2004**, *55*, 65−111.
(36) Little, S. H.; Sherman, D. M.; Vance, D.; Hein, J. R. Molecular controls on Cu and Zn isotopic fractionation in Fe-Mn crusts. *Earth Planet. Sci. Lett.* **2014**, *396*, 213−222.
(37) Fujii, T.; Moynier, F.; Telouk, P.; Abe, M. Experimental and theoretical investigation of isotope fractionation of zinc between aqua, chloro, and macrocyclic complexes. *J. Phys. Chem. A* **2010**, *114*, 2543−2552.
(38) Fujii, T.; Moynier, F.; Dauphas, N.; Abe, M. Theoretical and experimental investigation of nickel isotopic fractionation in species relevant to modern and ancient oceans. *Geochim. Cosmochim. Acta* **2011**, *75*, 469−482.
(39) Fujii, T.; Moynier, F.; Blichert-Toft, J.; Albarède, F. Density functional theory estimation of isotope fractionation of Fe, Ni, Cu, and Zn among species relevant to geochemical and biological environments. *Geochim. Cosmochim. Acta* **2014**, *140*, 553−576.
(40) Yin, H.; Tan, N.; Liu, C.; Wang, J.; Liang, X.; Qu, M.; Feng, X.; Qiu, G.; Tan, W.; Liu, F. The associations of heavy metals with crystalline iron oxides in the polluted soils around the mining areas in Guangdong Province, China. *Chemosphere* **2016**, *161*, 181−189.
(41) Cornell, R. M.; Schwertmann, U. *The Iron Oxides: Structure, Properties, Reactions, Occurences and Uses*; Wiley-VCH: Weinheim, 2003.
(42) Speight, J. G. *Lange's Handbook of Chemistry*, 16th ed.; McGraw Hill: Wyoming, 2005.
(43) Zhang, Y.; Wen, H.; Zhu, C.; Fan, H.; Cloquet, C. Cadmium isotopic evidence for the evolution of marine primary productivity and the biological extinction event during the Permian-Triassic crisis from the Meishan section, South China. *Chem. Geol.* **2018**, *481*, 110−118.
(44) Zhu, C.; Wen, H.; Zhang, Y.; Fan, H.; Fu, S.; Xu, J.; Qin, T. Characteristics of Cd isotopic compositions and their genetic significance in the lead-zinc deposits of SW China. *Sci. China Earth Sci.* **2013**, *56*, 2056−2065.
(45) Cloquet, C.; Rouxel, O.; Carignan, J.; Libourel, G. Natural cadmium isotopic variations in eight geological reference materials (NIST SRM 2711, BCR 176, GSS-1, GXR-1, GXR-2, GSD-12, Nod-P-1, Nod-A-1) and anthropogenic samples, measured by MC-ICP-MS. *Geostand. Geoanal. Res.* **2005**, *29*, 95−106.
(46) Zhang, Y.; Wen, H.; Zhu, C.; Fan, H.; Luo, C.; Liu, J.; Cloquet, C. Cd isotope fractionation during simulated and natural weathering. *Environ. Pollut.* **2016**, *216*, 9−17.
(47) Ravel, B.; Newville, M. ATHENA, ARTEMIS, HEPHAESTUS: data analysis for X-ray absorption spectroscopy using IFEFFIT. *J. Synchrotron Radiat.* **2005**, *12*, 537−541.
(48) Kelly, S. D.; Hesterberg, D.; Ravel, B. Analysis of soils and minerals using X-ray absorption spectroscopy. In *Methods of Soil Analysis, Part 5-Mineralogical Methods*; Ulrey, A. L., Drees, R. L., Eds.; Soil Science Society of America, 2008.
(49) Rehr, J. J.; Albers, R. C.; Zabinsky, S. I. High-order multiple-scattering calculations of x-ray-absorption fine structure. *Phys. Rev. Lett.* **1992**, *69*, 3397−3400.
(50) Sun, Q.; Cui, P.-X.; Zhu, M.; Fan, T.-T.; Ata-Ul-Karim, S. T.; Gu, J.-H.; Wu, S.; Zhou, D.-M.; Wang, Y.-J. Cd(II) retention and remobilization on $\delta$-$MnO_2$ and Mn(III)-rich $\delta$-$MnO_2$ affected by Mn(II). *Environ. Int.* **2019**, *130*, 104932.
(51) Teo, B. K. *EXAFS: Basic Principles and Data Analysis*; Springer Berlin Heidelberg, 2012.
(52) Bochatay, L.; Persson, P.; Sjöberg, S. Metal ion coordination at the water−manganite ($\gamma$-MnOOH) interface: I. An EXAFS study of cadmium(II). *J. Colloid Interface Sci.* **2000**, *229*, 584−592.
(53) Rout, K.; Mohapatra, M.; Anand, S. 2-line ferrihydrite: synthesis, characterization and its adsorption behaviour for removal of Pb(II), Cd(II), Cu(II) and Zn(II) from aqueous solutions. *Dalton Trans.* **2012**, *41*, 3302−3312.
(54) Jiang, W.; Lv, J.; Luo, L.; Yang, K.; Lin, Y.; Hu, F.; Zhang, J.; Zhang, S. Arsenate and cadmium co-adsorption and co-precipitation on goethite. *J. Hazard. Mater.* **2013**, *262*, 55−63.
(55) Li, W.; Zhang, S.; Jiang, W.; Shan, X.-q. Effect of phosphate on the adsorption of Cu and Cd on natural hematite. *Chemosphere* **2006**, *63*, 1235−1241.
(56) Boyanov, M. I.; Kelly, S. D.; Kemner, K. M.; Bunker, B. A.; Fein, J. B.; Fowle, D. A. Adsorption of cadmium to Bacillus subtilis bacterial cell walls: a pH-dependent X-ray absorption fine structure spectroscopy study. *Geochim. Cosmochim. Acta* **2003**, *67*, 3299−3311.
(57) Gräfe, M.; Mustafa, G.; Singh, B.; Kookana, R. S. Chapter 7 Temperature and Aging Effects on the Surface Speciation of Cd(II) at the Goethite−Water Interface. In *Developments in Earth and Environmental Sciences*; Barnett, M. O., Kent, D. B., Eds.; Elsevier, 2007; Vol. *7*, pp 187−204.
(58) Rietveld, H. M. A profile refinement method for nuclear and magnetic structures. *J. Appl. Crystallogr.* **1969**, *2*, 65−71.
(59) Huynh, T.; Tong, A. R.; Singh, B.; Kennedy, B. J. Cd-substituted goethites - A structural investigation by synchrotron X-ray diffraction. *Clays Clay Miner.* **2003**, *51*, 397−402.
(60) Kaur, N.; Gräfe, M.; Singh, B.; Kennedy, B. Simultaneous incorporation of Cr, Zn, Cd, and Pb in the goethite structure. *Clays Clay Miner.* **2009**, *57*, 234−250.
(61) Pokrovsky, O. S.; Viers, J.; Emnova, E. E.; Kompantseva, E. I.; Freydier, R. Copper isotope fractionation during its interaction with soil and aquatic microorganisms and metal oxy(hydr)oxides: Possible structural control. *Geochim. Cosmochim. Acta* **2008**, *72*, 1742−1757.
(62) Wilkins, R. G. Mechanisms of ligand replacement in octahedral nickel(II) complexes. *Acc. Chem. Res.* **1970**, *3*, 408−416.
(63) Wilkins, R. G. *Kinetics and Mechanism of Reactions of Transition Metal Complexes*; Wiley, 1991.
(64) Randall, S. R.; Sherman, D. M.; Ragnarsdottir, K. V.; Collins, C. R. The mechanism of cadmium surface complexation on iron oxyhydroxide minerals. *Geochim. Cosmochim. Acta* **1999**, *63*, 2971−2987.
(65) Boily, J.-F.; Sjöberg, S.; Persson, P. Structures and stabilities of Cd(II) and Cd(II)-phthalate complexes at the goethite/water interface. *Geochim. Cosmochim. Acta* **2005**, *69*, 3219−3235.
(66) Collins, C. R.; Ragnarsdottir, K. V.; Sherman, D. M. Effect of inorganic and organic ligands on the mechanism of cadmium sorption to goethite. *Geochim. Cosmochim. Acta* **1999**, *63*, 2989−3002.


https://doi.org/10.1021/acs.est.0c06927
*Environ. Sci. Technol.* 2021, 55, 11601−11611

(67) Barrón, V.; Torrent, J. Surface hydroxyl configuration of various crystal faces of hematite and goethite. *J. Colloid Interface Sci.* **1996**, *177*, 407−410.
(68) Villalobos, M.; Cheney, M. A.; Alcaraz-Cienfuegos, J. Goethite surface reactivity: II. A microscopic site-density model that describes its surface area-normalized variability. *J. Colloid Interface Sci.* **2009**, *336*, 412−422.
(69) Venema, P.; Hiemstra, T.; Weidler, P. G.; van Riemsdijk, W. H. Intrinsic proton affinity of reactive surface groups of metal (hydr)oxides: Application to iron (hydr)oxides. *J. Colloid Interface Sci.* **1998**, *198*, 282−295.
(70) Gustafsson, J. P. *Visual MINTEQ 3.1*; KTH (Royal Institute of Technology): Stockholm, Sweden, 2014.
(71) Sheng, A.; Liu, J.; Li, X.; Qafoku, O.; Collins, R. N.; Jones, A. M.; Pearce, C. I.; Wang, C.; Ni, J.; Lu, A.; Rosso, K. M. Labile Fe(III) from sorbed Fe(II) oxidation is the key intermediate in Fe(II)-catalyzed ferrihydrite transformation. *Geochim. Cosmochim. Acta* **2020**, *272*, 105−120.
(72) Sheng, A.; Li, X.; Arai, Y.; Ding, Y.; Rosso, K. M.; Liu, J. Citrate controls Fe(II)-catalyzed transformation of ferrihydrite by complexation of the labile Fe(III) intermediate. *Environ. Sci. Technol.* **2020**, *54*, 7309−7319.
(73) Clayton, R. E.; Hudson-Edwards, K. A.; Malinovsky, D.; Andersson, P. Fe isotope fractionation during the precipitation of ferrihydrite and transformation of ferrihydrite to goethite. *Mineral. Mag.* **2005**, *69*, 667−676.
(74) Guinoiseau, D.; Galer, S. J. G.; Abouchami, W.; Frank, M.; Achterberg, E. P.; Haug, G. H. Importance of cadmium sulfides for biogeochemical cycling of Cd and its isotopes in oxygen deficient zones—A case study of the Angola Basin. *Global Biogeochem. Cycles* **2019**, *33*, 1746−1763.
(75) Cloquet, C.; Carignan, J.; Libourel, G.; Sterckeman, T.; Perdrix, E. Tracing source pollution in soils using cadmium and lead isotopes. *Environ. Sci. Technol.* **2006**, *40*, 2525−2530.
(76) Wiggenhauser, M.; Bigalke, M.; Imseng, M.; Müller, M.; Keller, A.; Murphy, K.; Kreissig, K.; Rehkämper, M.; Wilcke, W.; Frossard, E. Cadmium isotope fractionation in soil-wheat systems. *Environ. Sci. Technol.* **2016**, *50*, 9223−9231.
(77) Zhong, Q.; Zhou, Y.; Tsang, D. C. W.; Liu, J.; Yang, X.; Yin, M.; Wu, S.; Wang, J.; Xiao, T.; Zhang, Z. Cadmium isotopes as tracers in environmental studies: A review. *Sci. Total Environ.* **2020**, *736*, 139585.


https://doi.org/10.1021/acs.est.0c06927
*Environ. Sci. Technol.* 2021, 55, 11601−11611